HHS Public Access

Author manuscript

Matrix Biol. Author manuscript; available in PMC 2018 July 01.

Published in final edited form as:

Matrix Biol. 2017 July ; 60-61: 70–85. doi:10.1016/j.matbio.2016.07.002.

Force regulated conformational change of integrin $\alpha_V\beta_3$

Yunfeng Chen[1,2], **Hyunjung Lee**[3], **Haibin Tong**[4,5], **Martin Schwartz**[4,6], and **Cheng Zhu**[1,2,3,*]

[1]Woodruff School of Mechanical Engineering, Georgia Institute of Technology, Atlanta, Georgia 30332, USA

[2]Petit Institute for Bioengineering and Biosciences, Georgia Institute of Technology, Atlanta, Georgia 30332, USA

[3]Coulter Department of Biomedical Engineering, Georgia Institute of Technology, Atlanta, Georgia 30332, USA

[4]Yale Cardiovascular Research Center, Departments of Internal Medicine (Section of Cardiovascular Medicine), Yale University, New Haven, Connecticut 06511, USA

[6]Depts of Cell Biology and Biomedical Engineering, Yale University, New Haven, Connecticut 06511, USA

Abstract

Integrins mediate cell adhesion to extracellular matrix and transduce signals bidirectionally across the membrane. Integrin $\alpha_V\beta_3$ has been shown to play an essential role in tumor metastasis, angiogenesis, hemostasis and phagocytosis. Integrins can take several conformations, including the bent and extended conformations of the ectodomain, which regulate integrin functions. Using a biomembrane force probe, we characterized the bending and unbending conformational changes of a single integrin $\alpha_V\beta_3$ molecule on a living cell surface in real-time. We measured the probabilities of conformational changes, rates and speeds of conformational transitions, and the dynamic equilibrium between the two conformations, which were regulated by tensile force, dependent on the ligand, and altered by point mutations. These findings provide insights into how $\alpha_V\beta_3$ acts as a molecular machine and how its physiological function and molecular structure are coupled at the single molecule level.

Keywords

biomechanics; integrin $\alpha_V\beta_3$; integrin conformational change; binding kinetics; force regulation

[*]Correspondence to Cheng Zhu: Coulter Department of Biomedical Engineering, Georgia Institute of Technology, Atlanta, Georgia 30332, USA. cheng.zhu@bme.gatech.edu.

[5]Current address: Life Science Research Center, Beihua University, Jilin 132013, China

Introduction

Integrin $\alpha_V\beta_3$ is a member of the integrin family and is widely expressed on endothelial cells, osteoclasts and blood cells. It acts as a bridging molecule between the cell and the extracellular environment, and mediates cell adhesions and mechanosignaling (Horton, 1997; Jiang et al., 2006; Roca-Cusachs et al., 2009). The over-expression of integrin $\alpha_V\beta_3$ in certain tumor cells facilitates tumor development, angiogenesis, and metastasis (Liu et al., 2008).

Integrins are heterodimers of non-covalently associated α and β subunits with an extracellular domain, a transmembrane segment, and a cytoplasmic region (Luo and Springer, 2006). Integrins can adopt multiple conformations, including a bent or extended ectodomain, a joined or separated tailpiece and a closed or opened β subunit hybrid domain, which have been visualized by electron microscopy and crystallography (Arnaout et al., 2005; Choi et al., 2013; Luo and Springer, 2006; Nishida et al., 2006; Xie et al., 2010; Xiong et al., 2009; Xiong et al., 2001) and detected by conformation-specific antibodies (Zhang et al., 2013). Specifically, integrin $\alpha_V\beta_3$, the subject of the present paper, has been observed in both bent and extended ectodomain conformations (Takagi et al., 2002; Xiong et al., 2009; Xiong et al., 2001). In the bent conformation, the N-terminal headpiece of the integrin (including the β-propeller and thigh domains of the α subunit and βA and hybrid domains of the β subunit) is bent towards and contacts the C-terminal tailpiece (including Calf-1 and Calf-2 domains of the α subunit and I-EGF-1 to I-EGF-4 domains and β tail domain of the β subunit). Upon extension, the headpiece flips upwards around the N-terminus of Calf-1 and I-EGF-1 domains and becomes more aligned with the tailpiece.

Integrin conformation is known to correlate with integrin activity: the bent conformation correlates with low affinity for ligands whereas the extended conformation correlates with high affinity. Integrin activation is accompanied by ectodomain extension, as shown by studies with extracellular activators, such as divalent cations (e.g. Mg^{2+}, Mn^{2+}), activating antibodies (e.g. CBR LFA1/2), and ligand-mimicking peptides, and with intracellular activators such as overexpressed talin head domain (Chen et al., 2010b; Nishida et al., 2006; Schurpf and Springer, 2011; Shattil et al., 2010; Takagi et al., 2002; Ye et al., 2012). Several activation-associated mutations also result in more extended conformations compared to the wild-type (WT) (Zhang et al., 2013). Molecular dynamics (MD) simulations have suggested that mechanical forces may induce integrin conformational changes (Chen et al., 2011; Puklin-Faucher et al., 2006; Saltel et al., 2009; Xiang et al., 2011; Zhu et al., 2008). Using a single-molecule force technique, the biomembrane force probe (BFP), we characterized bending and unbending conformational changes of a single integrin $\alpha_L\beta_2$ on a living cell, which has demonstrated a role for mechanical force to regulate integrin conformational changes (Chen et al., 2012).

Building upon these recent studies, here we used a BFP to investigate bending and unbending conformational changes of single $\alpha_V\beta_3$ integrins on living cells. Characterization of the conformational change dynamics revealed the effects of mutation, force and ligand engagement.

Results

Real-time observation of single integrin $\alpha_V\beta_3$ conformational changes on living cells

We used a BFP to characterize the conformational dynamics and binding kinetics of human integrin $\alpha_V\beta_3$ expressed on mouse lung endothelial cells (mLECs), including WT and two gain-of-function (GOF) mutants (MT), D723R and L138I (see Experimental Procedures). D723R, located at the N-terminus of the β_3 cytoplasmic domain (Fig. 1A), disrupts interactions between the α- and β-subunit transmembrane domain-tail to induce integrin tail separation and functional activation (Li et al., 2014; Pines et al., 2011; Tadokoro et al., 2003). L138I, a point mutation in the β_3 βA domain, promotes extracellular domain extension and also activates the integrin (Pines et al., 2011). Cells grown to confluence were detached from a culture flask by EDTA, washed, and injected into the cell chamber on the microscope stage. A mLEC was aspirated by the right micropipette and served as the target (Fig. 1B *right*). Two ligands and two anti-β_3 antibodies were tested. Most experiments used a biotinylated fibronectin module III domain 7-10 ($FN_{III7\text{-}10}$) containing both the integrin-binding RGD sequence in the domain 10 and the synergy site in the domain 9 (Petrie et al., 2010). The biotin-$FN_{III7\text{-}10}$ was immobilized on a streptavidin (SA) covalently coupled glass bead that served as the probe (Fig. 1B *left*). Some experiments used fibrinogen (Fg) or antibody covalently coupled to the probe bead together with SA for attachment to the biotinylated RBC (Fig. 1B *left*). The covalent linking protocol resulted in random distribution of non-clustered SA, Abs or Fg on the bead surface, an important condition to ensure binding events of different ligands to be independent and to follow the Poisson statistics at small numbers. Binding specificity was confirmed using the adhesion frequency as an assay (see Experimental Procedures). Target cells were driven to repeatedly contact the probe bead for 2 seconds then retracted, and the number of no-adhesion (Fig. 1C, ①) and adhesion (Fig. 1C, ②) events were counted. At appropriately adjusted ligand density, bead binding to mLECs expressing WT, D723R or L138I $\alpha_V\beta_3$ exhibited 30-40% frequencies; in comparison, binding to untransfected cells was ~five-fold lower, ensuring the observed binding events were predominately mediated by $\alpha_V\beta_3$ (Fig. 1D). Contacts between SA-bearing beads and mLECs expressing WT $\alpha_V\beta_3$ also yielded a very low level of adhesion frequency, confirming the binding specificity of the ligand $FN_{III7\text{-}10}$ (Fig. 1D).

Position-clamp experiments (see Experimental Procedures) were performed to quantify $\alpha_V\beta_3$–$FN_{III7\text{-}10}$ bond dissociation and the integrin bending and unbending conformational changes under force. The contact time was shortened to lower the adhesion frequency to ~20%, a necessary but not sufficient condition to ensure binding between the bead and the cell to be mediated predominately (~90%) by a single bond (Chesla et al., 1998). Upon retraction to a desired force level, the mLEC was clamped at a fixed position to allow measurement of the lifetimes of the bonds (if present) and observe the subsequent bending or unbending event. Under such a position-clamp condition, the force signal often remained stable around the initial value until dissociation (Fig. 1C, ③). The lifetime (Fig. 1C, indicated) reflects the sustainability of the bond at a given force. However, in some lifetime events, a spontaneous decrease (Fig. 2A and C) or increase (Fig. 2B and D) in the mean force signal was observed with a concurrent decrease (Fig. 2E) or increase (Fig. 2F) in their fluctuations, indicating that the integrin under interrogation underwent an unbending or

bending conformational change, respectively (Chen et al., 2012). The force change was due to the lengthening or shortening of the distance between the ligand-binding site and the membrane anchor point of the integrin, which partly decreased or increased pulling on the RBC, respectively. The change in the signal fluctuation results from the change in the integrin molecular stiffness, which is softer in the bent and stiffer in the extended conformation (See below) (Chen et al., 2012).

In rare cases the cell and the bead were linked by more than one bond. Because of the random distribution of $FN_{III7\text{-}10}$, these bonds tended to be spatially separated and formed independent from each other. As such, their dissociations during the clamping phase should occur independently, most likely one at a time rather than two or more simultaneously, resulting in sequential drops in the BFP force signal (Fig. 2G). Although Fig. 2A and G appear to look alike, a bond dissociation event could be distinguished from an unbending event by examining the corresponding fluctuations in the force signals. Dissociation would reduce the bond number, which would decrease the stiffness of the molecular linkage between the cell and the bead, thereby increasing the thermal fluctuation (Fig. 2I,K). This would be opposite to the thermal fluctuation decrease following integrin unbending. By the same token, the event of formation of an additional bond during clamping (Fig. 2H) appears to look alike the event of bending. But the two types of events could be distinguished by a decrease in the thermal fluctuation (Fig. 2J,L) due to an increase in the stiffness of the molecular linkage between the cell and the bead after bond formation. This again would be opposite to the thermal fluctuation increase following integrin bending. This criterion, explained in more detail below, was used to eliminate the rare multiple-bond events (~5%) and ensured single-bond resolution in our observation.

Characterizing bending and unbending events

Bending and unbending events were collected from >1,000 lifetime events for each $\alpha_V\beta_3$ construct over forces ranging from 0-45 pN (Fig. 3A, C, E, and G, Table 1). The displacements resulting from integrin bending (for WT only) and unbending (for WT, D723R and L138I) were narrowly distributed as single-peak Gaussians (Fig. 3B, D, F, and H). Note that the displacement distributions from bending of D723R and L138I were not available due to the rare occurrence of these events, which made displacement measurements impractical (Table 1). The average displacements of bending and unbending were comparable, showing no dependence on force (Fig. 3A, C, E, and G) and were indistinguishable for all of the integrin constructs (Fig. 3I). The ~15 nm average displacement values agree with the predicted distance changes of ligated $\alpha_V\beta_3$ unbending by MD simulations (Chen et al., 2011). The frequency of unbending events was much higher than that of bending events for all three integrin constructs, especially for the two GOF MTs for which bending events were rarely observed (Fig. 3J).

As controls, two antibodies (LIBS-2 and AP3) were coated onto the beads instead of $FN_{III7\text{-}10}$ to pull the integrins. The LIBS-2 epitope resides in the βTD domain, which is close to the transmembrane domain (Fig. 1A) (Byron et al., 2009; Mitchell et al., 2007). We therefore predicted that bending or unbending of $\alpha_V\beta_3$ should not result in displacement of the LIBS-2 epitope. Validating this prediction, signals resembling those of putative bending

or unbending events were not observed in 350 lifetime events (Fig. 3I and J; Table 1). The antigenic epitope of AP3, by comparison, resides at the PSI and hybrid domains that are part of the β_3 headpiece (Fig. 1A) and is therefore expected to move closer to or further away from the membrane as $\alpha_V\beta_3$ undergoes bending or unbending conformational change, respectively (Byron et al., 2009). Indeed, both unbending and bending events were observed from 371 lifetime events (Fig. 3J; Table 1). The bending and unbending displacements measured with AP3 were similar (~10 nm), smaller than those measured using $FN_{III7\text{-}10}$ (Fig. 3I), which is expected because the AP3 epitope is closer to the membrane than the $FN_{III7\text{-}10}$ binding site (Fig. 1A). These results confirm the authenticity of the observed bending and unbending events and suggest that ligand binding is not required to induce these events.

Analyzing force regulated integrin bending-unbending equilibrium

Under a pulling force, integrins can behave as a softer or stiffer spring, depending on whether they take an extended or bent conformation. This finding, reported for integrins $\alpha_L\beta_2$ (Chen et al., 2012) and $\alpha_4\beta_1$ (Choi et al., 2014), was also observed in this study for integrin $\alpha_V\beta_3$, as illustrated in Fig. 2. The fluctuation of the force signal represents thermal fluctuation of the force probe confined by an energy well defined by two springs in parallel – the RBC spring and the $\alpha_V\beta_3$–$FN_{III7\text{-}10}$ molecular spring. A softer $\alpha_V\beta_3$ spring relaxes the confinement, resulting in larger thermal fluctuation (Chen et al., 2008b; Marshall et al., 2006). Thus, the thermal fluctuation decreased after unbending (Fig. 2C and E) and increased after bending (Fig. 2D and F) (Chen et al., 2012).

The molecular stiffness of the $\alpha_V\beta_3$–$FN_{III7\text{-}10}$ complex was also measured by the stretch method (See Experimental Procedures) (Marshall et al., 2006), using the force vs. displacement curve in the retraction phase (cf. Fig. 1C). The slope in the compressive force regime represents the stiffness of the target cell (Fig. 4A, purple line; Fig. 4B); while the slope in the tensile force regime represents the overall stiffness of the target cell and the $\alpha_V\beta_3$–$FN_{III7\text{-}10}$ molecular complex in series (Fig. 4A, red line; Fig. 4B).

Note that molecular stiffness measurements provide diagnosis for multimeric bonds, as the higher the bond number, the stiffer the molecular linkage between the cell and the bead (Sarangapani et al., 2011). To confirm that our measurements represented mostly single bond events, we used a monomeric MT SA to capture the biotinylated $FN_{III7\text{-}10}$ onto the bead surface, which has only one binding site for biotin instead of four in the generally used tetrameric WT SA. This was to address the possible multimeric bonds between potentially up to four $FN_{III7\text{-}10}$ captured by a single WT SA and a cluster of $\alpha_V\beta_3$ (if integrins on mLECs were clustered). Multiple bonds between different $FN_{III7\text{-}10}$ captured on the same WT SA and integrins in a cluster might not form and dissociate independently due to their close proximity. This would negate our argument for single bond measurements based on Poisson distribution, because a force drop in the BFP signal might represent simultaneous dissociation of a multimeric bond instead of one of its member. The use of MT SA would eliminate such possibility. The average stiffness of the molecular complex with the WT and MT SA were indistinguishable (Fig. 4C), suggesting that multimeric bonds, if formed when WT SA was used, were negligible.

When we segregated the WT SA stiffness data into two groups based on whether a bending or unbending event was later observed in the position-clamp phase (cf. Fig. 1C), we found that within each group, the three integrin constructs were similarly stiff (Fig. 4D). As expected, the mean ± SEM stiffness values were significantly higher for the group measured before bending than the group measured before unbending for all three $\alpha_V\beta_3$ constructs (Fig. 4D). Histogram analysis showed a right-shift of the stiffness distribution of the group measured before bending relative to the group measured before unbending (Fig. 4E). Each histogram was well fitted by a Gaussian distribution (Fig. 4E, solid curves). This suggested that the adhesion events are dominated by single-molecule interactions, for otherwise each histogram should distribute as multiple Gaussians given that multiple bonds should have 2 or more times of the stiffness of a single bond, as we previously shown (Sarangapani et al., 2011). The mean values of the fitting, k_{bent} = 0.40 and $k_{extended}$ = 0.67 pN/nm, representing the average spring constants of a single $\alpha_V\beta_3$–$FN_{III7\text{-}10}$ bonding complex with the integrin in the bent and extended conformations, respectively.

The initial fractions of bent and extended integrin subpopulations reflect the equilibrium of the integrin conformations in the absence of force. To determine these parameters, distributions of molecular stiffness from all BFP test cycles with lifetime measurements (with and without bending or unbending events) were fitted by a dual Gaussian with two fixed means at 0.40 and 0.67 pN/nm. WT $\alpha_V\beta_3$ integrins were 55.8% bent and 44.2% extended in physiological medium (1 mM Ca^{2+} and 1 mM Mg^{2+}), while the activated MTs, D723R and L138I, had higher fractions in the extended form (Fig. 4F-H).

To determine the probability for an extended integrin to bend under a pulling force exerted through an engaged ligand, we normalized the observed frequency of bending events (Fig. 3J) by the initial fraction of extended integrin. Similarly, we calculated the probability of unbending by dividing the number of unbending events by the number of lifetime events from initially bent integrins (Table 1). The probability of a WT bent integrin to unbend was similar to that of L138I, whereas D723R had a nearly two-fold higher unbending probability of D723R, suggesting that the D723R mutation facilitates unbending. On the other hand, the respective probabilities of an extended D723R and L138I integrin to bend were similar but ≥35-fold lower than that of WT, indicating that bending was significantly suppressed by the two mutations (Table 1). Note that because the length of lifetime events determines the time window of observation for conformational changes, the bond lifetime differences among WT, D723R and L138I may also contribute to the aforementioned probability differences.

When the bent and extended integrin conformations reach a dynamic equilibrium, the following equation should hold: (Extended fraction)*(Bending rate) = (Bent fraction)*(Unbending rate). Thus:

$$\frac{(\text{Extended fraction})}{(\text{Bent fraction})}=\frac{(\text{Unbending rate})}{(\text{Bending rate})} \quad \text{Equation 1}$$

In our BFP experiment, a pulling force was exerted on the molecular complex. It seems reasonable to predict that force would facilitate unbending and suppress bending, thus

inducing a shift of the conformational equilibrium towards extension. To validate this prediction, the fractions of extended and bent integrins under force were estimated. Because (Probability of unbending)/(Probability of bending) = (Unbending rate)/(Bending rate), following Equation 1 we have (Extended fraction)/(Bent fraction) = (Probability of unbending)/(Probability of bending). Based on this equation and the respective probabilities of unbending and bending in Table 1, we derived the overall equilibrium state of WT (33.0% bent, 67.0% extended), D723R (0.6% bent, 99.4% extended) and L138I (1.4% bent, 98.6% extended) under all forces. Comparing these numbers to those under zero-force (Table 1, Bent fraction and Extended fraction) revealed that the equilibrium was drastically shifted towards the extended state under force.

Analyzing force regulated integrin bending-unbending dynamics

To derive the dynamics of integrin conformational changes, we measured the switching time ($t_{sw\pm}$, defined in Fig. 2C and D) and times-to-switch ($t_{0\pm}$, defined in Fig. 2A and B) of unbending and bending events, which characterize the speed of conformational changes and the stability of conformations, respectively. WT unbending t_{sw+} and t_{0+} were both much shorter than the respective bending t_{sw-} and t_{0-} (Fig. 5A and B), likely due to force pulling on the integrin that facilitates unbending and suppresses bending. The unbending t_{sw+} values of D723R and L138I were similar but significantly shorter compared to that of WT. For the two mutants, bending events were too rare to obtain reliable t_{sw-} and t_{0-} measurements (Fig. 5A and B). D723R, not L138I, exhibited a shortened unbending t_{0+} compared to the WT (Fig. 5B). These data suggest that both mutations accelerated integrin unbending but only D723R destabilized the bent conformation.

To quantify the force regulation of integrin conformational changes, we segregated $t_{sw\pm}$ and $t_{0\pm}$ into a range of force bins. As predicted, increasing force monotonically shortened both the unbending t_{sw+} and t_{0+} of all three integrin constructs (Fig. 5C and D), consistent with our previous results on $\alpha_L\beta_2$ conformational changes (Chen et al., 2012). However, unlike our previous work where the bending t_{sw-} and t_{0-} for $\alpha_L\beta_2$ increased with force monotonically, the bending t_{sw-} and t_{0-} curves for the WT $\alpha_V\beta_3$ were biphasic, increasing with force until ~20 pN, and decreasing as force further increased (Fig. 5C and D). We speculate that this is owing to the potential constraints of the receptor–ligand bond lifetime on the observable t_{sw-} and t_{0-}: the bending or unbending events were observed only when they occurred prior to bond dissociation. Should the characteristic time scales of bending and bond dissociation be comparable, the t_{sw-} and t_{0-} measurements would be subject to selective sampling based on the occurrence of those bending events prior to bond dissociation, which would be biased towards smaller values. Indeed, the $\alpha_V\beta_3$–$FN_{III7\text{-}10}$ lifetime (Fig. 5E) was at the same scale as t_{sw-} and t_{0-} under all forces studied. More importantly, the average lifetime vs. force curve also behaved as a catch-slip bond with 0-20 pN being the “catch” regime, consistent with the t_{sw-} and t_{0-} vs. force curves.

Note that bond lifetime measurements provide another diagnosis for multimeric bonds, as the higher the bond number the longer the lifetime (Marshall et al., 2003). However, the average lifetimes of $\alpha_V\beta_3$ bonds with $FN_{III7\text{-}10}$ captured by WT and MT SA were

indistinguishable under both 25 and 50 pN (Fig. 5E), again indicating that multimeric bonds did not form in experiments using WT SA.

In the previous section, tensile force was shown to shift the conformation equilibrium towards extension. However, whether this was sensitive to the magnitude of force still needed to be confirmed. Because the ratio of time-to-unbend to time-to-bend is the reciprocal of the ratio of unbending rate to bending rate, Equation 1 can be converted to:

$$\frac{(\text{Bent fraction})}{(\text{Extended fraction})}=\frac{t_{0+}}{t_{0-}} \quad \text{Equation 2}$$

showing that the ratio t_{0+}/t_{0-} directly reflects the equilibrium between extended and bent conformations. Thus, the WT $\alpha_V\beta_3$ t_{0+}/t_{0-} ratio was plotted vs. force, exhibiting clear force-dependence (Fig. 5F, filled circles). The zero-force value was calculated from the fraction ratio of the extended to bent integrin sub-populations estimated in Fig. 4F according to Equation 2, which well matches the zero-force extrapolation from the points under force (Fig. 5F, open circle). Under all forces studied, the t_{0+}/t_{0-} ratio monotonically decreased with increasing force, indicating that the conformational equilibrium was gradually shifted towards extension (Fig. 5F).

Observing bending and unbending conformational changes of fibrinogen-bound WT $\alpha_V\beta_3$

We noted that the probabilities of WT $\alpha_V\beta_3$ bending and unbending conformational changes when the integrin was pulled by AP3 were much lower than those by $FN_{III7\text{-}10}$. This observation raised the possibility that these conformational changes may be ligand-dependent. To test this hypothesis, Fg, another ligand for $\alpha_V\beta_3$, was used to interrogate WT $\alpha_V\beta_3$. We observed both bending and unbending events with respective displacements distributed as single-peak Gaussians (Fig. 6A-D). Both the average bending and unbending displacements were ~15 nm, identical to those of $FN_{III7\text{-}10}$-bound $\alpha_V\beta_3$ (Fig. 3I). However, the probabilities of bending and unbending of the Fg-bound $\alpha_V\beta_3$ were slightly lower than those of the $FN_{III7\text{-}10}$-bound $\alpha_V\beta_3$ (p-value = 0.074 and 0.0008 respectively based on statistical comparison; Fig. 3J and Table 1), suggesting that Fg may favor less bending and unbending conformational changes.

Similar to $FN_{III7\text{-}10}$-bound $\alpha_V\beta_3$, the stiffness of Fg-bound $\alpha_V\beta_3$ also manifested a single Gaussian distribution before unbending instead of a broad and multi-peak histogram, suggesting that we observed predominately single $\alpha_V\beta_3$–Fg bonds (Fig. 6E). Due to the small number of bending events collected from Fg binding, their stiffness histogram analysis was not performed.

The unbending t_{sw+} of Fg-bound $\alpha_V\beta_3$ was comparable to that of $FN_{III7\text{-}10}$-bound $\alpha_V\beta_3$ (compare Fig. 5C and Fig. 6F, both curves with magenta solid squares), but the unbending t_{0+} values were slightly longer under all forces studied (compare Fig. 5D and Fig. 6G, both curves with magenta solid squares), which may partially explain the lower probability of unbending. On the other hand, the bending t_{sw-} of Fg-bound $\alpha_V\beta_3$ was longer than that of $FN_{III7\text{-}10}$-bound $\alpha_V\beta_3$ (compare Fig. 5C and Fig. 6F, both curves with magenta open

circles), while the bending t_{0-} values were comparable at lower forces but shorter at higher forces (compare Fig. 5D and Fig. 6G, both curves with magenta open circles).

Discussion

Integrins play a key role in sensing the mechanical stiffness of the extracellular matrix and external forces applied through the matrix. In both cases, magnitude and time courses of the forces affect cellular signaling pathways and outcomes. Available evidence suggests that multiple components of the physical linkage between the matrix ligands and the F-actin contribute to mechanosensing, to a large part through force-regulated conformation changes. Understanding how forces across integrins modulate conformational transitions is therefore an important goal.

It has long been proposed that integrins are constantly undergoing reversible conformational changes on living cells with a dynamic equilibrium determined by extracellular stimuli and intracellular activation (Campbell and Humphries, 2011). Recently, one pair of such dynamic conformational changes has been observed – the bending and unbending of $\alpha_L\beta_2$ (Chen et al., 2012). In the present work, we observed the bending and unbending conformational changes of $\alpha_V\beta_3$ on single-molecule scale, which differs structurally from $\alpha_L\beta_2$ in that α_L contains an αA domain whereas α_V does not.

In principle, our approach to ensuring the observed BFP signals to represent single-molecule event is similar to the generally accepted approach in the field of single-molecule force spectroscopy, both of which are based on molecular elasticity. Single molecule researchers usually add to the ligand a linker of known mechanical characteristic when subjected to force, referred to as a molecular fingerprint. Data that exhibit such a molecular fingerprint would be included, otherwise would be excluded. Commonly used linker includes an RNA or DNA hairpin that would unzip at a known force (Ritort, 2006), a poly(ethylene-glycol) polymer whose force-extension curve would follow the freely jointed chain model (Manibog et al., 2014), or a protein domain (e.g. titin I27 module) that would unfold at a known force with a saw-tooth patterned extension curve well characterized by the worm-like chain model (Serquera et al., 2010). By comparison, we used the differential stiffness of the bent and extended integrin themselves as molecular signatures. Our rationale for not using the linker approach is two-fold. First, the mechanical behavior of integrin's anchor to the cell (via transmembrane polypeptides and connection to the cytoskeleton via adaptor proteins) is complex and uncharacterized, which would likely mask the molecular fingerprint of the linker. Second, the objective of the present work is to characterize the integrin bending and unbending via analysis of the small change in the stiffness of the integrin–ligand complex due to integrin conformational changes. Adding another soft linker to the serially connected molecules (integrin and ligand) will decrease the relative change in the system stiffness due to integrin conformational change, therefore greatly reducing the measurement accuracy.

Bending and unbending were observed in $\alpha_V\beta_3$ when interrogated by two ligands, fibronectin fragment $FN_{III7\text{-}10}$ and Fg, as well as by antibody AP3 that targets an epitope outside the ligand-bind site. Our approach for ensuring the observed BFP force signals represents single integrin bending and unbending is to identify the signatures of the said

molecular events. As pointed out by our previous paper (Chen et al., 2012), possible sources of noise signals include: 1) formation of an additional bond or dissociation of a bond from a multi-bond adhesion; 2) instrument drift; 3) cell deformation/movement; 4) membrane extrusion and 5) protein unfolding and refolding. Because molecules can be modeled as elastic mechanically, under clamping forces the receptor–ligand complex is elongated. The elongated distance between the two surfaces should discourage the formation of addition bonds between molecules of their unstretched lengths. We used the concurrent changes in the mean and fluctuating force signals to distinguish the bending and unbending events from bond formation and dissociation events (Fig. 2). Unbending is signified by a decrease in the mean force and thermal fluctuation (increase in the integrin's head-to-tail distance and the molecular stiffness), while bending is signified by an increase in the mean force and thermal fluctuation (decrease in the integrin's head-to-tail distance and molecular stiffness). By comparison, formation of an additional bond is signified by an increase in the mean force and a decrease in thermal fluctuation (decrease in the distance between the cell and bead and stiffens the molecular linkage between them), while dissociation of a bond from a multi-bond adhesion is signified by an increase in the mean force and thermal fluctuation (increase in the distance between the cell and bead and softens the molecular linkage between them). We thus removed the bond formation and dissociation data from further analysis.

Moreover, we noted that manipulations of the biological system resulted in changes in our measurements that were consistent with changes in the integrin conformations that are known to be specific for such manipulations. For example, we tested two GOF mutants (L138I and D723R) expected to favor unbending but suppress bending. Both mutants significantly lowered the frequency of bending and shortened the unbending switching time; D723R enhanced the frequency of unbending and shortened the unbending time-to-switch (Fig. 5, Table 1). Replacing the ligands with the antibody LIBS-2 (which binds to the β_3 EGF-4 domain) eliminated all putative unbending and bending signatures from BFP signals, while antibody AP3 (which binds to the integrin head) resulted in less frequent putative unbending and bending signatures than $FN_{III7\text{-}10}$ and Fg (Fig. 3J). The same mLECs were used to express WT and MT integrin $\alpha_V\beta_3$, which should have felt the same force regardless of the integrin sites where forces were applied and responded in the same way, and the same BFP instrument was used to run experiments under identical physical conditions, which are not expected to change the measurements. These arguments ruled out non-specific factors such as instrument drift, cell deformation/movement and membrane tether extrusion in response to force as possible causes for the specific changes in the data. In addition, cell deformation/movement and membrane extrusion likely are in a much larger scale than the 15 nm displacement for $FN_{III7\text{-}10}$ and Fg and the 9.5 nm for AP3 (Fig. 3I). Previously, no domain unfolding and refolding in integrins have been reported. Protein unfolding usually requires larger forces than the majority of forces used in our studies (as low as ~5 pN). By comparison, extensive structural data show that integrins exist in bent and extended conformers, which can change back and forth on the cell surface to carry out different functions in response to environmental conditions and cell signaling. Thus, bending and unbending seem to be a far more reasonable explanation for our data than domain unfolding and refolding.

Frequencies of both bending and unbending events observed with $FN_{III7\text{-}10}$ and Fg, although higher than those with AP3, did show substantial differences (Fig. 3J). This suggests that the dynamic bending and unbending switches of an integrin, while could be influenced by, does not rely on ligand engagement, and may even occur without ligand association. The influence of ligand was also observed in the force regulated dynamics of conformational changes by the differences between the $t_{sw\pm}$ and $t_{0\pm}$ vs. force curves obtained for $FN_{III7\text{-}10}$- and Fg-bound integrins (Fig. 5C and D; Fig. 6F,G). Note that the synergy site in $FN_{III7\text{-}10}$ has trivial effect to $\alpha_V\beta_3$ binding (Bowditch et al., 1994), and that $\alpha_V\beta_3$ engages the same RGD motif in both ligands (Springer et al., 2008). Therefore, we suspect this ligand dependency of bending and unbending may be related to the distinctive docking caused by the adjacent sequences of the $FN_{III7\text{-}10}$ and Fg RGD motifs, which may produce different allosteric effects that propagate from the N-terminal ligand binding region to the overall structure of the integrin. These effects are likely to contribute to the differential cellular responses to mechanical stresses observed in cells on different matrix proteins (Atance et al., 2004; Collins et al., 2014; Seong et al., 2013).

Similar to our previous results (Chen et al., 2012), the average displacements due to integrin bending and unbending show no dependence on force. The reason is that these displacements represent changes in head-to-tail distance of integrin. As such, they are determined by the integrin structure rather than the force-elongation relationship that underlies the molecular stiffness. Integrin bending and unbending are not mechanical processes of elastic deformation in which the molecule's length behaves as a smooth increasing function of force. Instead, they can be thought of as kinetic processes of state transition in which the integrin conformation switches between two stable conformations: bent and extended conformers. The integrin head-to-tail distance can increase (during unbending) and decrease (during bending) at any force (within a range). Force mainly regulates the rates of state transitions (i.e., force-dependent $t_{0\pm}$ as shown in Figs. 5B, 5D and 6G). Thus, although force can also affect the lengths of the two conformers that can be treated as elastic bodies, the length changes due to elastic response of the two stable conformers are expected to be small compared with those due to conformational changes.

The corresponding criteria for distinguishing bending and unbending events from BFP force signals are spontaneous increase and decrease of the mean force with concurrent decrease and increase of the force fluctuation. The mean force change is a direct readout of the displacement of the integrin head toward or away from the cell membrane. The change in force fluctuation is due to the stiffness difference in bent and extended conformations of the integrin. To confirm that, we measured the respective molecular spring constants of the $\alpha_V\beta_3$–ligand complex before bending or unbending events, which reflect the relative stiffness of the integrin in the extended or bent conformations. Similar to previous results with $\alpha_L\beta_2$ (Chen et al., 2012), we found the integrin $\alpha_V\beta_3$ is also softer in the bent and stiffer in the extended conformation (Fig. 4D). Histogram analysis allowed us to determine the initial fractions of bent and extended integrin sub-populations in the absence of force (Fig. 4F-H).

Mutagenesis has been utilized to analyze integrin activity and signaling (Flevaris et al., 2007; Pines et al., 2011). The GOF mutation L138I, which is located in the ectodomain head

piece, results in a higher fraction of extended integrins than the WT (Fig. 4H), consistent with its reported function (Pines et al., 2011). This effect correlates with a shorter switching time for the bent to unbent conformational transition (Fig 5A), whereas the time delay before undergoing the switch was the same as WT (Fig 5B). Interestingly, D723R, which causes tailpiece separation, promotes extension more strongly (Fig. 4G). This correlates with an effect on switching time, which was the same as L138I, but with shortening the time to switch as well (Fig. 5D). This result suggests that α–β tail separation represents a distinct barrier to unbending that can be rate limiting. The effect of the D723R mutation also dramatically demonstrates the long range allosteric relay of the conformational change (Pines et al., 2011). Indeed, the switching time is very long compared to other protein conformational transitions (Hammes, 2002; Husada et al., 2015), indicating a complex energy profile with multiple steps.

Mechanical force regulates integrin conformational changes by providing or requiring energy as the headpiece moves along or against the direction of force. Intuitively, one would expect tensile force exerted via engaged ligand to impede bending and favor unbending. Indeed, we found $t_{sw-} >> t_{sw+}$ and $t_{0-} >> t_{0+}$ (Fig. 5A and B). Also, both t_{sw+} and t_{0+} decrease with force, and t_{sw-} and t_{0-} increase with force until 20 pN beyond which rapid ligand dissociation limits the measurement of long t_{sw-} and t_{0-} values (Fig. 5C and D). These data indicate that force accelerates unbending, decelerates bending, stabilizes the extended state, and destabilizes the bent state. As a result, force tilts the dynamic equilibrium towards more extended and less bent conformations.

Catch bonds have been found on several integrins interacting with their ligands (Chen et al., 2010a; Choi et al., 2014; Fiore et al., 2014; Kong et al., 2009; Rosetti et al., 2015). A recent work demonstrated the catch-bond behavior of a soluble integrin $\alpha_V\beta_3$ binding to $FN_{III7\text{-}10}$ (Elosegui-Artola et al., 2016), which is consistent with the present result of cell surface $\alpha_V\beta_3$ (Fig. 5E).

Integrin $\alpha_V\beta_3$ has been shown to initiate cell mechanotransduction via ligand engagement (Roca-Cusachs et al., 2009; Wang and Ha, 2013). However, the detailed process remains elusive. Although it is generally thought that integrin bending and unbending conformational changes contribute to signal transduction (Hynes, 2002), how physical forces affect these processes is poorly understood. Force-regulated integrin bending and unbending conformational changes could serve as triggering events and induce additional conformational changes downstream, e.g., rearrangements in the juxtamembrane domains (Deng and Li, 2015). Future studies will explore such intriguing possibilities.

Experimental Procedures

Proteins and reagents

Biotinylated $FN_{III7\text{-}10}$ was a gift from Dr. Andres Garcia (Georgia Tech, GA). Human plasma fibrinogen was a gift from Dr. Shaun Jackson (The University of Sydney, Australia). The antibody AP3 was a generous gift from Dr. Peter Newman (Blood Center of Wisconsin, WI). The antibody LIBS-2 was purchased from EMD Millipore (Billerica, MA). The anti-mouse β1 blocking Ab HMβ1-1 was purchased from Biolegend (San Diego, CA).

MAL-PEG3500-NHS and Biotin-PEG3500-NHS were purchased from JenKem (Plano, TX). Nystatin, streptavidin–maleimide and BSA were purchased from Sigma-Aldrich (St. Louis, MO). Borosilicate glass beads were purchased from Distrilab Particle Technology (RC Leusden, The Netherlands).

Cell lines

β3 null mouse lung endothelial cells (mLECs) isolated from the lungs of $\beta3^{-/-}$ mice and immortalized by retroviral delivery of a SV40 large T antigen essentially as described (Liao et al., 2015) were generously provided by Mark Ginsberg and Brian Petrich (University of California at San Diego, CA). β3 WT, D723R and L138I human integrin cDNAs, gifts from Mark Ginsberg and Timothy Springer (Harvard Medical School, Boston, MA), were cloned into pBOB, packaged into lentivirus and used to infect the immortalized β3 null mLECs as described (Coon et al., 2015). Reconstituted cell lines were FACS sorted to obtain cell populations with equivalent integrin surface levels. All mLECs were maintained in a 1:1 mixture of DMEM low glucose:Ham's F12 nutrient mixture (Invitrogen) supplemented with 0.05 mg/ml ECGS (Endothelial Cell Growth Factor) (from BD Biosciences), 0.1 mg/ml heparin and 10% Heat inactivated FBS. Cells were routinely checked by flow cytometry for surface expression of ICAM2 and PECAM1 to ensure they retained their normal EC characteristics throughout culture.

RBC and glass bead preparation

8-10 μl of human blood was obtained from finger prick abiding a protocol approved by the Institutional Review Board of Georgia Institute of Technology, and RBCs were isolated by centrifugation and biotinylated by incubating with Biotin-PEG3500-NHS solution (Chen et al., 2015; Rosetti et al., 2015). The biotinylated RBCs were then incubated with nystatin, which would swell the RBCs to near spherical shapes.

The functionalization of beads has been described previously (Chen et al., 2015). Glass beads were first thiolated. To make $FN_{III7\text{-}10}$ beads, the thiolated glass beads were incubated with streptavidin–maleimide, and then biotinylated $FN_{III7\text{-}10}$. To coat Fg, LIBS-2 or AP3 on beads, the protein of interest was first linked to MAL-PEG3500-NHS (JenKem), and then incubated with the thiolated glass beads. All beads after incubation were washed with and resuspended in phosphate buffer (27.6 g/L $NaH_2PO_4 \cdot H_2O$, 28.4 g/L Na_2HPO_4).

BFP setup and experiment modes

The BFP apparatus has been described in previous works (Chen et al., 2012; Chen et al., 2015; Fiore et al., 2014). A chamber was filled with cell culture medium (Low glucose DMEM, Hams F-12, heparin, glutamine, Pen/strep, Heat inactivated FBS, Endothelial Cell Growth Factor). 1% BSA and 1mM Ca^{2+}/Mg^{2+} were added to block non-specific binding and maintain a physiological cation condition, respectively. An anti-mouse β_1 Ab (HMβ1-1) was added to block the function of β_1 integrins originally expressed on the mLECs. A biotinylated RBC was aspirated by a micropipette to act as a force transducer (Fig. 1B). On the apex of the RBC was a probe bead attached via SA-biotin interaction (Fig. 1B). The bead was functionalized with proteins of interest to interact with the integrins on the target cell (Fig. 1B). A mLEC was aspirated by an opposing micropipette (Fig. 1B), which was driven

by a piezoelectric translator (Physical Instrument) with a feedback control. The probe bead position was tracked by an inverted microscope (Nikon TiE, Nikon) through two cameras with 3 nm precision in real-time. Data was analyzed with LabView (National Instrument).

The RBC spring constant k was determined as described (Chen et al., 2008a; Evans et al., 1995). k was set to 0.3 pN/nm or 0.25 pN/nm for clamping forces higher or lower than 10 pN, respectively.

Adhesion frequency experiment—An adhesion frequency assay reports the two-dimensional (2D) binding strength between two surfaces (Chen et al., 2015; Chesla et al., 1998). The target cell was driven to approach and contact the probe bead at a given contact time (2 sec in Fig. 1C) and retract. An adhesion was signified by a tensile force signal (②, Fig. 1C), while a no-adhesion was manifested by the force directly returning to zero (①, Fig. 1C). The approach-contact-retraction cycle was repeated for 50 times with 4 cell-bead pairs to yield an average adhesion frequency.

Position-clamp experiment—The target cell was driven repeatedly to contact and impinge the probe bead to form a receptor/ligand bond. The target pipette was then retracted at 3μm/s. In the binding events that survived the retraction phase, the target pipette was held at a desired position (reflected by the initial clamping force) to wait for the bond to dissociate, and then returned to the original position to start the next cycle (③, Fig. 1C). Lifetime was defined as from the instant when the force reached the desired level to the instant of bond dissociation (Fig. 1C, indicated). The probe-target contact time was adjusted to keep the adhesion infrequent (<20%), which is necessary for mostly (> 89%) single bonds (Chen et al., 2010a; Chesla et al., 1998).

Lifetime analysis

Lifetime data were categorized into bins of successive force ranges under which lifetimes were measured. The average lifetime in each force bin was collected to plot the lifetime curve as a function of force.

Measurements of molecular stiffness

Stretch method as previously described was used to measure the molecular stiffness (Chen et al., 2012). The retraction phase from the BFP “force vs. time” signal was converted to “force vs. displacement” (Fig. 4A), in which the displacement was calculated as the differential displacement between the BFP tracking system and the piezoelectric actuator feedback system. A tensile force pulled on the serially linked cell and the receptor-ligand molecular complex. Therefore, the reciprocal of the system stiffness equaled the sum of the reciprocals of the stiffness of the cell and the molecular complex. It was assumed that the molecular complex can resist tension but not compression, and that the target cell has the same stiffness under compressive or tensile force (Chen et al., 2012). Thus, Equation 3 was established to calculate the stiffness of the molecular complex:

$$\begin{cases} \frac{1}{\text{Slope}_1} = \frac{1}{k_{\text{cell}}} \\ \frac{1}{\text{Slope}_2} = \frac{1}{k_{\text{cell}}} + \frac{1}{k_{mol}} \end{cases} \quad \text{Equation 3}$$

in which $Slope_1$ and $Slope_2$ were the slopes of the linear fits to the "force vs. displacement" curve segments under compression (purple dashed line) and tension (red dashed line), respectively (Fig. 4A). k_{cell} and k_{mol} were the stiffness of the cell and the molecular complex, respectively.

Acknowledgements

We thank A. Garcia (Georgia Institute of Technology, Atlanta, GA) for $FN_{III7\text{-}10}$, P. J. Newman (BloodCenter of Wisconsin, Milwaukee, WI) for antibody AP3, and S. Jackson (The University of Sydney, Sydney, Australia) for fibrinogen.

This work was supported by National Institutes of Health grant R01AI044902 (CZ), and the Army Research Office MURI W911NF-14-0403.

Abbreviations

Ab	antibody
BFP	biomembrane force probe
BSA	bovine serum albumin
Fg	fibrinogen
FNIII7-10	fibronectin module III domain 7-10
GOF	Gain-of-function
MT	mutant
SA	streptavidin
WT	wild type

References

Arnaout MA, Mahalingam B, Xiong JP. Integrin structure, allostery, and bidirectional signaling. Annual review of cell and developmental biology. 2005; 21:381–410.

Atance J, Yost MJ, Carver W. Influence of the extracellular matrix on the regulation of cardiac fibroblast behavior by mechanical stretch. Journal of cellular physiology. 2004; 200:377–386. [PubMed: 15254965]

Bowditch RD, Hariharan M, Tominna EF, Smith JW, Yamada KM, Getzoff ED, Ginsberg MH. Identification of a novel integrin binding site in fibronectin. Differential utilization by beta 3 integrins. The Journal of biological chemistry. 1994; 269:10856–10863. [PubMed: 7511609]

Byron A, Humphries JD, Askari JA, Craig SE, Mould AP, Humphries MJ. Anti-integrin monoclonal antibodies. J Cell Sci. 2009; 122:4009–4011. [PubMed: 19910492]

Campbell ID, Humphries MJ. Integrin structure, activation, and interactions. Cold Spring Harbor perspectives in biology. 2011; 3

Chen W, Evans EA, McEver RP, Zhu C. Monitoring receptor-ligand interactions between surfaces by thermal fluctuations. Biophysical journal. 2008a; 94:694–701. [PubMed: 17890399]

Chen W, Lou J, Evans EA, Zhu C. Observing force-regulated conformational changes and ligand dissociation from a single integrin on cells. The Journal of cell biology. 2012; 199:497–512. [PubMed: 23109670]

Chen W, Lou J, Hsin J, Schulten K, Harvey SC, Zhu C. Molecular dynamics simulations of forced unbending of integrin alpha(v)beta(3). PLoS computational biology. 2011; 7:e1001086. [PubMed: 21379327]

Chen W, Lou J, Zhu C. Forcing switch from short- to intermediate- and long-lived states of the alphaA domain generates LFA-1/ICAM-1 catch bonds. The Journal of biological chemistry. 2010a; 285:35967–35978. [PubMed: 20819952]

Chen W, Zarnitsyna VI, Sarangapani KK, Huang J, Zhu C. Measuring Receptor-Ligand Binding Kinetics on Cell Surfaces: From Adhesion Frequency to Thermal Fluctuation Methods. Cellular and molecular bioengineering. 2008b; 1:276–288. [PubMed: 19890486]

Chen X, Xie C, Nishida N, Li Z, Walz T, Springer TA. Requirement of open headpiece conformation for activation of leukocyte integrin alphaXbeta2. Proceedings of the National Academy of Sciences of the United States of America. 2010b; 107:14727–14732. [PubMed: 20679211]

Chen Y, Liu B, Ju L, Hong J, Ji Q, Chen W, Zhu C. Fluorescence Biomembrane Force Probe: Concurrent Quantitation of Receptor-ligand Kinetics and Binding-induced Intracellular Signaling on a Single Cell. Journal of visualized experiments: JoVE. 2015

Chesla SE, Selvaraj P, Zhu C. Measuring two-dimensional receptor-ligand binding kinetics by micropipette. Biophysical journal. 1998; 75:1553–1572. [PubMed: 9726957]

Choi WS, Rice WJ, Stokes DL, Coller BS. Three-dimensional reconstruction of intact human integrin alphaIIbbeta3: new implications for activation-dependent ligand binding. Blood. 2013; 122:4165–4171. [PubMed: 24136164]

Choi YI, Duke-Cohan JS, Chen W, Liu B, Rossy J, Tabarin T, Ju L, Gui J, Gaus K, Zhu C, Reinherz EL. Dynamic control of beta1 integrin adhesion by the plexinD1-sema3E axis. Proceedings of the National Academy of Sciences of the United States of America. 2014; 111:379–384. [PubMed: 24344262]

Collins C, Osborne LD, Guilluy C, Chen Z, O'Brien ET 3rd, Reader JS, Burridge K, Superfine R, Tzima E. Haemodynamic and extracellular matrix cues regulate the mechanical phenotype and stiffness of aortic endothelial cells. Nature communications. 2014; 5:3984.

Coon BG, Baeyens N, Han J, Budatha M, Ross TD, Fang JS, Yun S, Thomas JL, Schwartz MA. Intramembrane binding of VE-cadherin to VEGFR2 and VEGFR3 assembles the endothelial mechanosensory complex. The Journal of cell biology. 2015; 208:975–986. [PubMed: 25800053]

Deng W, Li R. Juxtamembrane contribution to transmembrane signaling. Biopolymers. 2015

Elosegui-Artola A, Oria R, Chen Y, Kosmalska A, Pérez-González C, Castro N, Zhu C, Trepat X, Roca-Cusachs P. Mechanical regulation of a molecular clutch defines force transmission and transduction in response to matrix rigidity. Nature cell biology. 2016

Evans E, Ritchie K, Merkel R. Sensitive force technique to probe molecular adhesion and structural linkages at biological interfaces. Biophysical journal. 1995; 68:2580–2587. [PubMed: 7647261]

Fiore VF, Ju L, Chen Y, Zhu C, Barker TH. Dynamic catch of a Thy-1-alpha5beta1+syndecan-4 trimolecular complex. Nature communications. 2014; 5:4886.

Flevaris P, Stojanovic A, Gong H, Chishti A, Welch E, Du X. A molecular switch that controls cell spreading and retraction. The Journal of cell biology. 2007; 179:553–565. [PubMed: 17967945]

Hammes GG. Multiple conformational changes in enzyme catalysis. Biochemistry-Us. 2002; 41:8221–8228.

Horton MA. The alpha v beta 3 integrin "vitronectin receptor". The international journal of biochemistry & cell biology. 1997; 29:721–725. [PubMed: 9251239]

Husada F, Gouridis G, Vietrov R, Schuurman-Wolters GK, Ploetz E, de Boer M, Poolman B, Cordes T. Watching conformational dynamics of ABC transporters with single-molecule tools. Biochemical Society transactions. 2015; 43:1041–1047. [PubMed: 26517920]

Hynes RO. Integrins: bidirectional, allosteric signaling machines. Cell. 2002; 110:673–687. [PubMed: 12297042]

Jiang G, Huang AH, Cai Y, Tanase M, Sheetz MP. Rigidity sensing at the leading edge through alphavbeta3 integrins and RPTPalpha. Biophysical journal. 2006; 90:1804–1809. [PubMed: 16339875]

Kong F, Garcia AJ, Mould AP, Humphries MJ, Zhu C. Demonstration of catch bonds between an integrin and its ligand. The Journal of cell biology. 2009; 185:1275–1284. [PubMed: 19564406]

Li A, Guo Q, Kim C, Hu W, Ye F. Integrin alphaII b tail distal of GFFKR participates in inside-out alphaII b beta3 activation. Journal of thrombosis and haemostasis: JTH. 2014; 12:1145–1155. [PubMed: 24837519]

Liao Z, Kato H, Pandey M, Cantor JM, Ablooglu AJ, Ginsberg MH, Shattil SJ. Interaction of kindlin-2 with integrin beta3 promotes outside-in signaling responses by the alphaVbeta3 vitronectin receptor. Blood. 2015; 125:1995–2004. [PubMed: 25587038]

Liu Z, Wang F, Chen X. Integrin alpha(v)beta(3)-Targeted Cancer Therapy. Drug development research. 2008; 69:329–339. [PubMed: 20628538]

Luo BH, Springer TA. Integrin structures and conformational signaling. Current opinion in cell biology. 2006; 18:579–586. [PubMed: 16904883]

Manibog K, Li H, Rakshit S, Sivasankar S. Resolving the molecular mechanism of cadherin catch bond formation. Nature communications. 2014; 5:3941.

Marshall BT, Long M, Piper JW, Yago T, McEver RP, Zhu C. Direct observation of catch bonds involving cell-adhesion molecules. Nature. 2003; 423:190–193. [PubMed: 12736689]

Marshall BT, Sarangapani KK, Wu J, Lawrence MB, McEver RP, Zhu C. Measuring molecular elasticity by atomic force microscope cantilever fluctuations. Biophysical journal. 2006; 90:681–692. [PubMed: 16258054]

Mitchell WB, Li J, Murcia M, Valentin N, Newman PJ, Coller BS. Mapping early conformational changes in alphaIIb and beta3 during biogenesis reveals a potential mechanism for alphaIIbbeta3 adopting its bent conformation. Blood. 2007; 109:3725–3732. [PubMed: 17209052]

Nishida N, Xie C, Shimaoka M, Cheng Y, Walz T, Springer TA. Activation of leukocyte beta2 integrins by conversion from bent to extended conformations. Immunity. 2006; 25:583–594. [PubMed: 17045822]

Petrie TA, Raynor JE, Dumbauld DW, Lee TT, Jagtap S, Templeman KL, Collard DM, Garcia AJ. Multivalent integrin-specific ligands enhance tissue healing and biomaterial integration. Science translational medicine. 2010; 2:45ra60.

Pines M, Fairchild MJ, Tanentzapf G. Distinct regulatory mechanisms control integrin adhesive processes during tissue morphogenesis. Developmental dynamics: an official publication of the American Association of Anatomists. 2011; 240:36–51. [PubMed: 21089076]

Puklin-Faucher E, Gao M, Schulten K, Vogel V. How the headpiece hinge angle is opened: New insights into the dynamics of integrin activation. The Journal of cell biology. 2006; 175:349–360. [PubMed: 17060501]

Ritort F. Single-molecule experiments in biological physics: methods and applications. Journal of physics. Condensed matter: an Institute of Physics journal. 2006; 18:R531–583. [PubMed: 21690856]

Roca-Cusachs P, Gauthier NC, Del Rio A, Sheetz MP. Clustering of alpha(5)beta(1) integrins determines adhesion strength whereas alpha(v)beta(3) and talin enable mechanotransduction. Proceedings of the National Academy of Sciences of the United States of America. 2009; 106:16245–16250. [PubMed: 19805288]

Rosetti F, Chen Y, Sen M, Thayer E, Azcutia V, Herter JM, Luscinskas FW, Cullere X, Zhu C, Mayadas TN. A Lupus-Associated Mac-1 Variant Has Defects in Integrin Allostery and Interaction with Ligands under Force. Cell Rep. 2015

Saltel F, Mortier E, Hytonen VP, Jacquier MC, Zimmermann P, Vogel V, Liu W, Wehrle-Haller B. New PI(4,5)P2- and membrane proximal integrin-binding motifs in the talin head control beta3-integrin clustering. The Journal of cell biology. 2009; 187:715–731. [PubMed: 19948488]

Sarangapani KK, Marshall BT, McEver RP, Zhu C. Molecular stiffness of selectins. The Journal of biological chemistry. 2011; 286:9567–9576. [PubMed: 21216951]

Schurpf T, Springer TA. Regulation of integrin affinity on cell surfaces. The EMBO journal. 2011; 30:4712–4727. [PubMed: 21946563]

Seong J, Tajik A, Sun J, Guan JL, Humphries MJ, Craig SE, Shekaran A, Garcia AJ, Lu S, Lin MZ, Wang N, Wang Y. Distinct biophysical mechanisms of focal adhesion kinase mechanoactivation by different extracellular matrix proteins. Proceedings of the National Academy of Sciences of the United States of America. 2013; 110:19372–19377. [PubMed: 24222685]

Serquera D, Lee W, Settanni G, Marszalek PE, Paci E, Itzhaki LS. Mechanical unfolding of an ankyrin repeat protein. Biophysical journal. 2010; 98:1294–1301. [PubMed: 20371329]

Shattil SJ, Kim C, Ginsberg MH. The final steps of integrin activation: the end game. Nature reviews. Molecular cell biology. 2010; 11:288–300. [PubMed: 20308986]

Springer TA, Zhu J, Xiao T. Structural basis for distinctive recognition of fibrinogen gammaC peptide by the platelet integrin alphaIIbbeta3. The Journal of cell biology. 2008; 182:791–800. [PubMed: 18710925]

Tadokoro S, Shattil SJ, Eto K, Tai V, Liddington RC, de Pereda JM, Ginsberg MH, Calderwood DA. Talin binding to integrin beta tails: a final common step in integrin activation. Science. 2003; 302:103–106. [PubMed: 14526080]

Takagi J, Petre BM, Walz T, Springer TA. Global conformational rearrangements in integrin extracellular domains in outside-in and inside-out signaling. Cell. 2002; 110:599–511. [PubMed: 12230977]

Wang X, Ha T. Defining single molecular forces required to activate integrin and notch signaling. Science. 2013; 340:991–994. [PubMed: 23704575]

Xiang X, Lee CY, Li T, Chen W, Lou J, Zhu C. Structural basis and kinetics of force-induced conformational changes of an alphaA domain-containing integrin. PloS one. 2011; 6:e27946. [PubMed: 22140490]

Xie C, Zhu J, Chen X, Mi L, Nishida N, Springer TA. Structure of an integrin with an alphaI domain, complement receptor type 4. The EMBO journal. 2010; 29:666–679. [PubMed: 20033057]

Xiong JP, Mahalingham B, Alonso JL, Borrelli LA, Rui X, Anand S, Hyman BT, Rysiok T, Muller-Pompalla D, Goodman SL, Arnaout MA. Crystal structure of the complete integrin alphaVbeta3 ectodomain plus an alpha/beta transmembrane fragment. The Journal of cell biology. 2009; 186:589–600. [PubMed: 19704023]

Xiong JP, Stehle T, Diefenbach B, Zhang R, Dunker R, Scott DL, Joachimiak A, Goodman SL, Arnaout MA. Crystal structure of the extracellular segment of integrin alpha Vbeta3. Science. 2001; 294:339–345. [PubMed: 11546839]

Ye F, Kim C, Ginsberg MH. Reconstruction of integrin activation. Blood. 2012; 119:26–33. [PubMed: 21921044]

Zhang C, Liu J, Jiang X, Haydar N, Zhang C, Shan H, Zhu J. Modulation of integrin activation and signaling by alpha1/alpha1'-helix unbending at the junction. J Cell Sci. 2013; 126:5735–5747. [PubMed: 24144695]

Zhu J, Luo BH, Xiao T, Zhang C, Nishida N, Springer TA. Structure of a complete integrin ectodomain in a physiologic resting state and activation and deactivation by applied forces. Molecular cell. 2008; 32:849–861. [PubMed: 19111664]

Highlights

Integrins mediate cell adhesion to extracellular matrix and transduce signals bidirectionally across the membrane. Integrins can take several conformations, including the bent and extended conformations of the ectodomain, which regulate its functions. Using a biomembrane force probe, we characterized the bending and unbending conformational changes of a single integrin $\alpha_V\beta_3$ molecule on a living cell surface in real-time.

It was found that the bending and unbending conformational changes of $\alpha_V\beta_3$ do not require ligand binding to occur. However, the binding of ligands, including a fibronectin fragment and fibrinogen, influences the probabilities of conformational changes as well as rates and speeds of conformational transitions. Agreeing with a previous paper, the average displacements due to integrin bending and unbending show no dependence on force, and the molecular stiffness of the integrin is higher when extended and lower when bent. Two gain-of-function mutants, D723R and L138I, facilitate the process of unbending, and result in a higher fraction of extended integrins than the WT. Mechanical force provides energy that favors unbending and discourages bending, and thus accelerates unbending, decelerates bending, stabilizes the extended state, and destabilizes the bent state.

Integrin $\alpha_V\beta_3$ initiates cell mechanotransduction, which is thought to be related to the bending and unbending conformational changes. Our findings provide insights into how $\alpha_V\beta_3$ acts as a molecular machine and how its physiological function and molecular structure are coupled at the single molecule level.

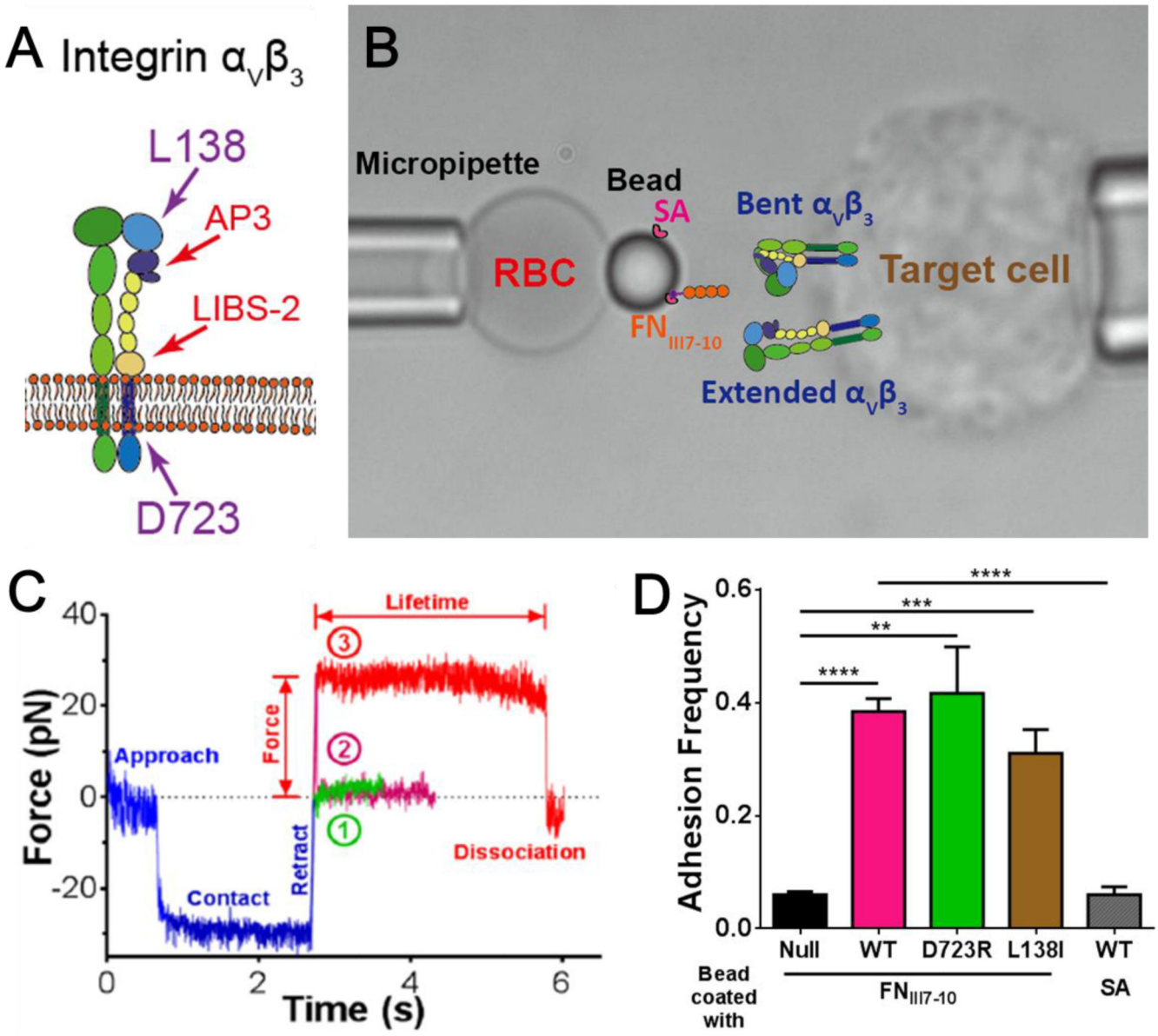

Figure 1.

BFP assay and specificity test. (A) Cartoon of integrin $\alpha_V\beta_3$. The position of two residues L138 and D723 and the epitopes of two antibodies AP3 and LIBS-2 were indicated by arrowheads. (B) BFP photomicrograph. A bead was attached to the apex of a micropipette-aspirated red blood cell (RBC, left) to form a force probe. The probe was aligned against a mouse lung endothelial cell (mLEC, target cell, right) aspirated by an apposing micropipette. Drawn on the bead and the mLEC: BFP functionalization. The probe bead was pre-coated with streptavidin (SA) covalently, and incubated with N-terminally biotinylated fibronectin fragment $FN_{III7-10}$. The mLEC was transfected to express human integrin $\alpha_V\beta_3$. (C) Superimposition of three representative force vs. time traces from BFP test cycles. The target cell was driven to approach the probe bead, contacted for 2s with ~30pN of compressive force, and retracted. The force would return to zero as the compression was

relieved if there was no adhesion (①, green), or became positive if adhesion was present (②,③). The adhesion was either ruptured during the force-ramp phase signified by a force drop to zero (②, magenta), or survived the force-ramp to a pre-set force to be held constant (③, red, 25 pN as shown) until dissociation. The duration of such a force-clamp phase was measured as the bond lifetime. (D) Binding specificity tests. Adhesion frequencies between the $FN_{III7\text{-}10}$ bearing probe and cells expressing no (black), WT (magenta), D723R (green) or L138I (brown) integrin $\alpha_V\beta_3$, and between the SA bearing probe and cells expressing WT integrin (gray). Each probe–target pair was tested repeatedly for 50 cycles to estimate an adhesion frequency. Four probe–target pairs were tested to obtain mean ± SEM. ** = $p < 0.01$; *** = $p < 0.001$; **** = $p < 0.0001$, assessed by unpaired, two-tailed Student's t-test.

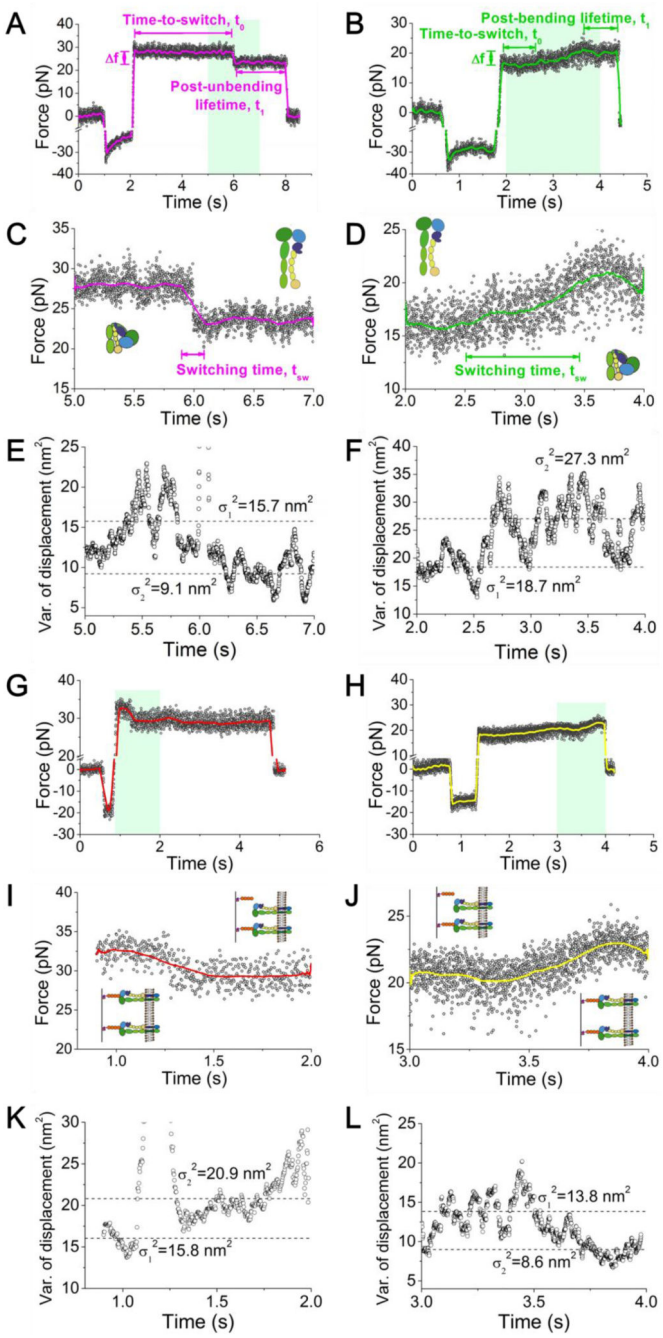

Figure 2.

BFP force signals of position-clamp $\alpha_V\beta_3$ unbending (A,C,E) and bending (B,D,F) conformational change events, and breakage (G,I,K) and formation (H,J,L) of an addition bond. (A-D) Representative force vs. time data showing a putative integrin unbending (A, C), and bending (B, D) event. A higher force resolution was obtained by smoothing the raw data using the Savitzky-Golay method (curves). Force changes (Δf), switching time ($t_{sw\pm}$), and time-to-switch ($t_{0\pm}$) are indicated. (A,B) The overall signals of BFP cycles that contain an integrin unbending (A) or bending (B) event. (C,D) The zoom-in views of the BFP

signals within the cyan-shaded time windows indicated in panel (A) or (B), which include the conformational changes of interest. The putative integrin global conformations were depicted by the cartoons before and after the said changes. (E,F) 100-point sliding variance of the displacement in (C) and (D) versus time. A decrease (E) or increase (F) in the thermal fluctuation (from σ_1^2 to σ_2^2, dashed lines) followed integrin unbending or bending, indicating the stiffening or softening of the integrin molecule, respectively. (G-J) Representative force vs. time data showing the dissociation of a bond from a two-bond adhesion (G, I) and formation (H, J) of an additional bond. A higher force resolution was obtained by smoothing the raw data using the Savitzky-Golay method (curves). (G,H) The overall signals of BFP cycles that contain an additional bond dissociation (G) or formation (H) event. (I,J) The zoom-in views of the BFP signals within the cyan-shaded time windows indicated in panel (G) or (H), which include the additional bond dissociation or formation. (K,L) 100-point sliding variance of the displacement in (I) and (J) versus time. An increase (K) or decrease (L) in the thermal fluctuation (from σ_1^2 to σ_2^2, dashed lines) followed bond dissociation or formation, indicating the weakening or strengthening of the linkage between the two surfaces, respectively.

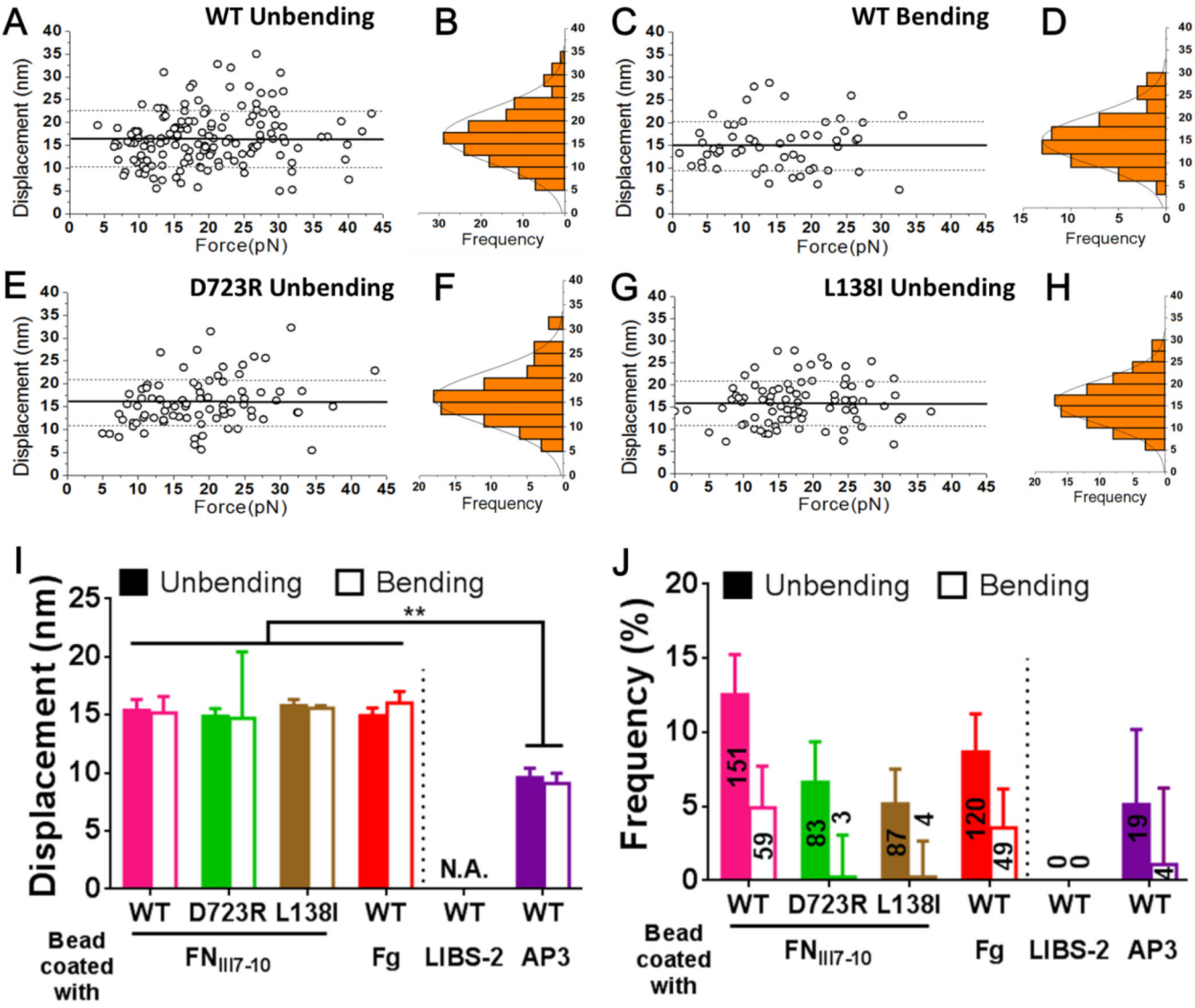

Figure 3.

Characterization of the bending and unbending events. (A,C,E,G) Scatter plots of displacement (= $\Delta f/k_{BFP}$ where the Δf measurement) was shown in Fig. 2, A and B and k_{BFP} = 0.3 pN/nm is the preset spring constant of the RBC) vs. pre-switch force of unbending (A,E,G) and bending (C) events of WT (A,C), D723R (E) and L138I (G) $\alpha_V\beta_3$ pulled via an engaged $FN_{III7\text{-}10}$. Mean ± SD of displacements are shown as solid and dashed lines. (B,D,F,H) Histograms (bars) and Gaussian fits (curves) of the data from A, C, E, and G. (I,J) Displacement (I, means ± SEM) and frequency (J, error bar = SEM estimated by the binomial distribution of events whose numbers are indicated) of unbending (filled bar) and bending (empty bar) of indicated $\alpha_V\beta_3$ pulled by different ligands ($FN_{III7\text{-}10}$, Fg)/antibodies (LIBS-2, AP3). ** = $p < 0.01$, assessed by unpaired, two-tailed Student's t-test. N.A. = not applicable due to lack of data.

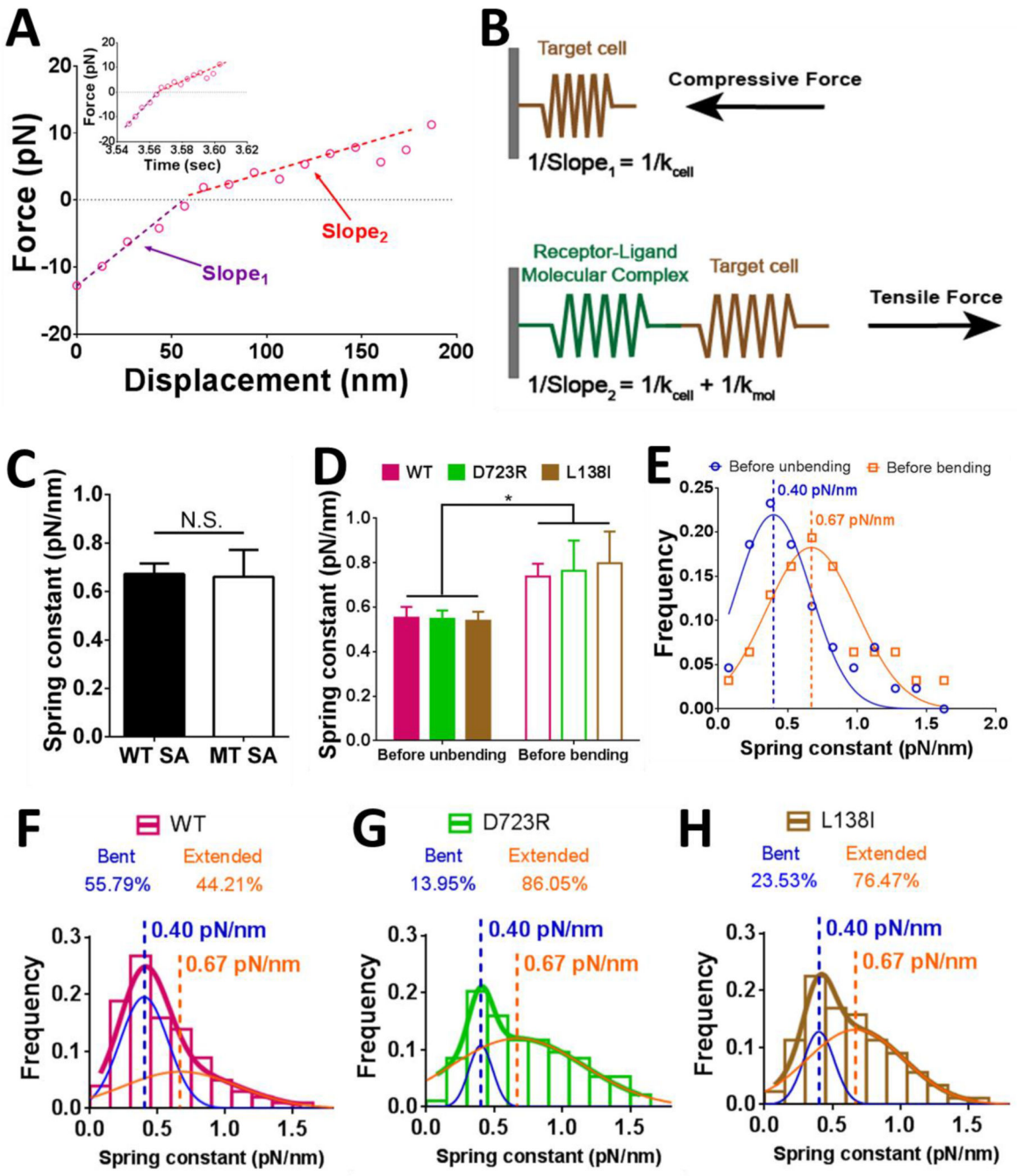

Figure 4.

Determining the molecular stiffness with a bent or extended integrin and the initial fractions of integrin populations in bent and extended conformations. (A) Force vs. displacement plot converted from a representative BFP force vs. time signal (insert). Two slopes can be clearly discerned in the piecewise linear curve, with the kink right on force = 0 (dashed line). (B) A schematic illustrating the slope calculations with the system under a compressive (upper) or tensile (lower) force. $Slope_1$ and $Slope_2$ were defined in panel (A). The equations of slope calculations were shown in corresponding panels. (C) Mean ± SEM of spring constants of

the molecular complex (k_{mol}) formed between WT $\alpha_V\beta_3$ and $FN_{III7\text{-}10}$ captured by tetrameric (WT, filled bar) and monomeric (MT, open bar) SA were compared. N.S. = not significant, assessed by unpaired, two-tailed Student's t-test. (D) Mean ± SEM of spring constants of the molecular complex (k_{mol}) prior to unbending (filled bars) or bending (empty bars) of the indicated integrin. * = $p < 0.05$, assessed by unpaired, two-tailed Student's t-test. (E) Data (points) and Gaussian fits (curves) of k_{mol} distributions measured from the ramping phase of BFP cycles with lifetime events during which integrin unbending (blue) or bending (orange) was observed in the clamping phase. The means of the two Gaussian distributions were indicated by dashed lines with the values annotated. Data from WT, D723R and L138I were pooled together, assuming that the two mutations had negligible effects in the integrin stiffness, as suggested by panel (D). (F-H) Histograms (bars) and dual Gaussian fits (blue and orange curves were fits to the two sub-populations; color-matched curves were fits to the whole populations) of k_{mol} for WT (F), D723R (G) and L138I (H) $\alpha_V\beta_3$ pulled by $FN_{III7\text{-}10}$. The calculated fractions of bent and extended sub-populations returned from the dual Gaussian fitting were indicated in each panel.

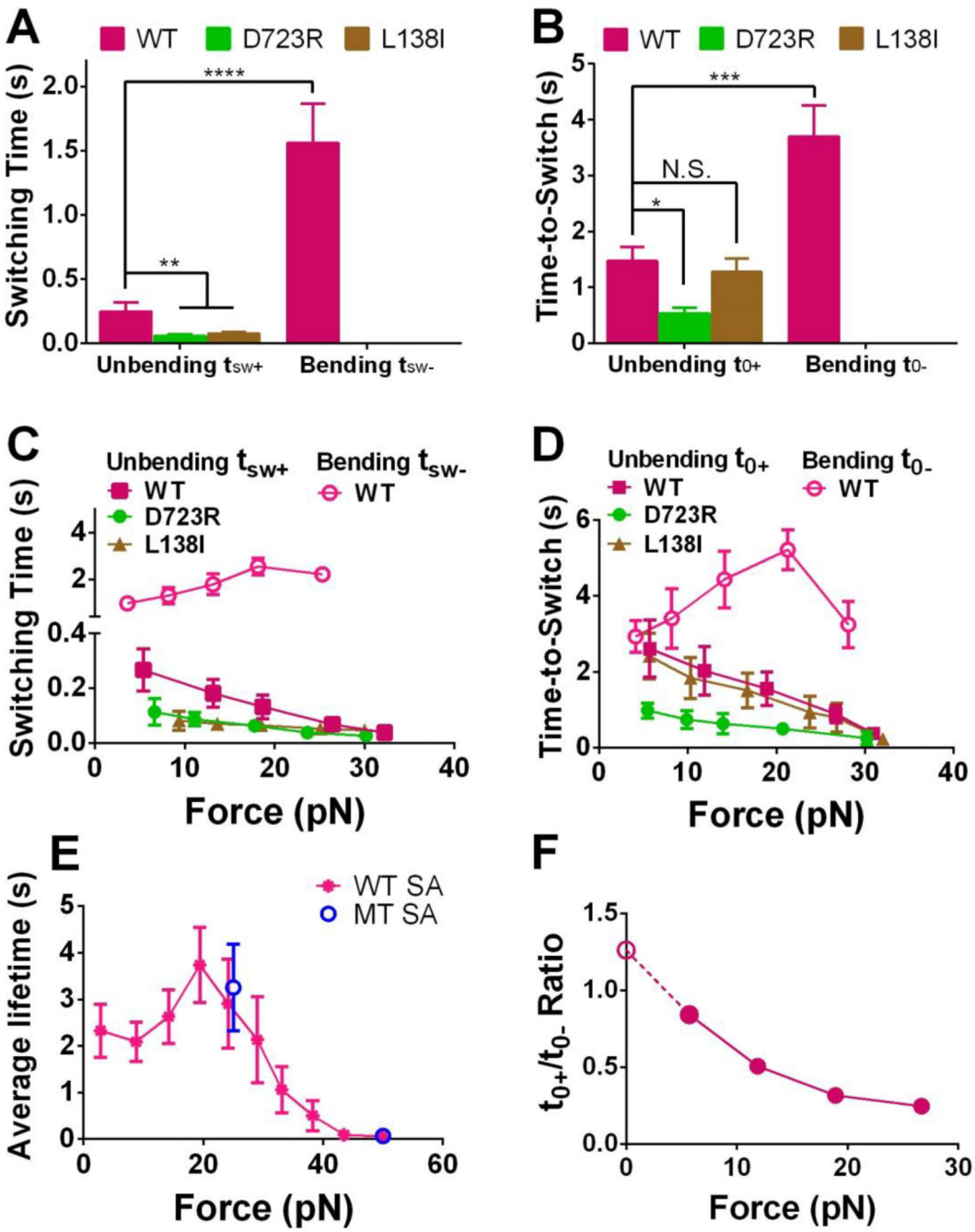

Figure 5.

Analyzing the dynamics of the integrin conformational changes. (A,B) Mean ± SEM of the switching time ($t_{sw\pm}$, A) or time-to-switch ($t_{0\pm}$, B) averaged over all clamping forces. (C,D) Bending (open symbols) and unbending (filled symbols) $t_{sw\pm}$ (C) or $t_{0\pm}$ (D) vs. pre-switch force curves for indicated integrins (Mean ± SEM). In A-D, bending of D723R and L138I $\alpha_V\beta_3$ occurred too infrequently to obtain sufficient data for statistically stable characterization thus were not summarized. (E) WT $\alpha_V\beta_3$-$FN_{III7\text{-}10}$ lifetime vs. force data from measurements not containing bending and unbending events, to show the potential

constraints of the receptor–ligand bond lifetime to the observable $t_{sw\pm}$ (C) and $t_{0\pm}$ (D). Lifetimes of WT $\alpha_V\beta_3$ bonds with $FN_{III7\text{-}10}$ captured by monomeric SA (MT, blue) at 25 and 50 pN were compared to those by tetrameric SA (WT, magenta) over an entire force range. (F) Ratio of WT $\alpha_V\beta_3$ time-to-unbend t_{0+} to time-to-bend t_{0-} vs. clamping force, showing the force-dependent bent/extended state equilibrium. The solid circles were calculated from data in panel D. The value of the open circle was the ratio of the extended to bent integrin sub-populations estimated from Fig. 4F. N.S. = not significant; * = $p < 0.05$; ** = $p < 0.01$; *** = $p < 0.001$ **** = $p < 0.0001$, assessed by unpaired, two-tailed Student's t-test.

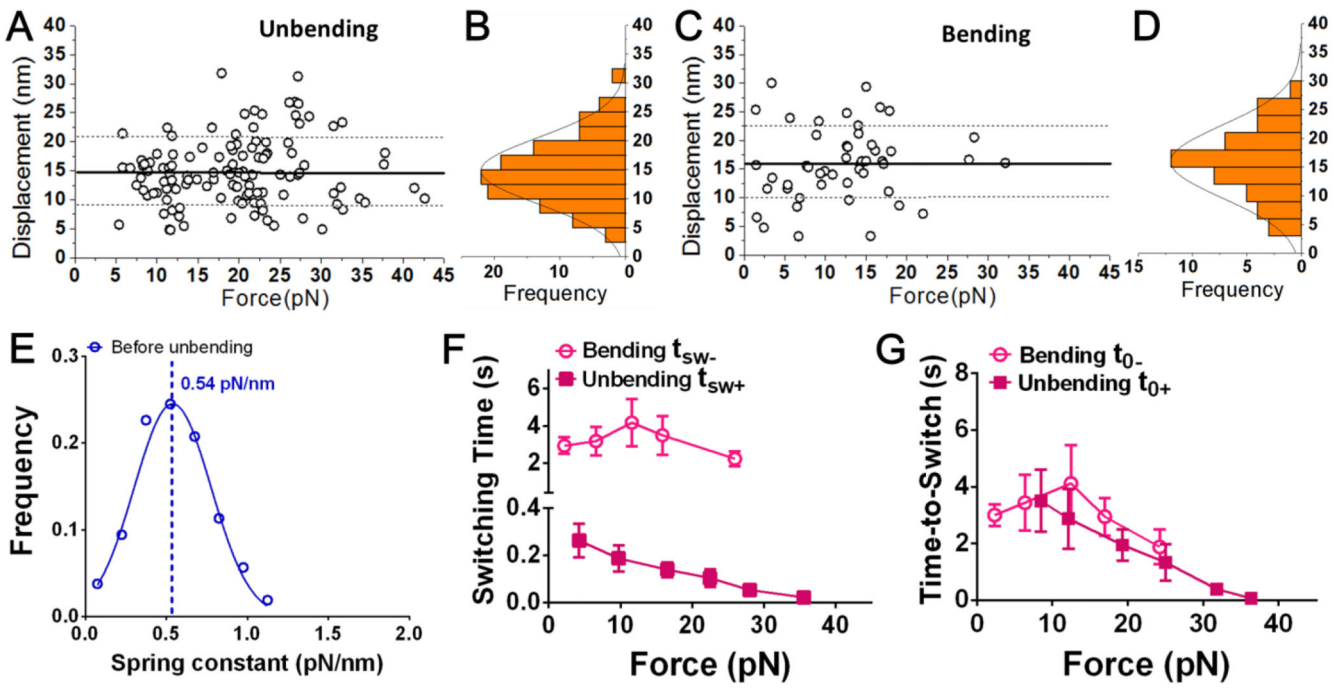

Figure 6.

Bending and unbending conformational changes of fibrinogen-bound WT $\alpha_V\beta_3$. (A,C) Scatter plots of displacement vs. pre-switch force of the unbending (A) and bending (C) events. Mean ± SD of displacements are shown as solid and dashed lines. (B,D) Histograms (bars) and Gaussian fits (curves) of the data from A and C. (E) Data (points) and Gaussian fit (curve) of k_{mol} distribution measured from the ramping phase of BFP cycles during which integrin unbending was observed in the clamping phase. The mean of the Gaussian distribution was indicated by a dashed line with the value annotated. (F,G) Bending and unbending switching $t_{sw\pm}$ (F) or $t_{0\pm}$ (G) vs. pre-switch force curves (Mean ± SEM).

Table 1

Statistics of total lifetime events measured and the bending/unbending conformational change events observed in BFP position-clamp experiments. The fractions of the bent and extended sub-populations of WT, D723R and L138I $\alpha_V\beta_3$ integrins were initial fractions derived from the fitting results in Fig. 4(E-G). Probability of unbending is calculated by (#Unbending events) / [(#Lifetime events) * (Bent fraction)]. Probability of bending is calculated by (#Bending events) / [(#Lifetime events) * (Extended fraction)].

Bead coated with	Phenotype	#Lifetime events	Bent fraction	Extended fraction	Unbending		Bending	
					#Events	Probability	#Events	Probability
$FN_{III7-10}$	WT	1203	55.79%	44.21%	151	22.50%	59	11.09%
	D723R	1252	13.95%	86.05%	83	47.52%	3	0.28%
	L138I	1685	23.53%	76.47%	87	21.94%	4	0.31%
Fibrinogen	WT	1384	55.79%	44.21%	120	15.54%	49	8.01%
LIBS-2		350			0	0.00%	0	0.00%
AP3		371			19	9.18%	4	2.44%